Mem. S.A.It. Suppl. Vol. 1, 165

Memorie della
Supplementi

A third order shock-capturing code for relativistic 3-D MHD

L. Del Zanna[1], N. Bucciantini[1], and P. Londrillo[2]

[1] Dipartimento di Astronomia e Scienza dello Spazio, Università degli Studi di Firenze, Largo E. Fermi 2, 50125 Firenze

[2] INAF, Osservatorio Astronomico di Bologna, Via C. Ranzani 1, 40127 Bologna

Abstract. A third order shock-capturing numerical scheme for three-dimensional special relativistic magnetohydrodynamics (3-D RMHD) is presented and validated against several numerical tests of astrophysical interest. The scheme avoids completely spectral decomposition into characteristic waves, computationally expensive and subject to many degenerate cases in the magnetic case, while it makes use of a two-speed Riemann solver that just require the knowledge of the two local fast magnetosonic velocities. Moreover, the onset of spurious magnetic monopoles, which is a typical problem for multi-dimensional MHD upwind codes, is prevented by properly taking into account the solenoidal constraint and the specific antisymmetric nature of the induction equation. The extension to generalized orthogonal curvilinear coordinate systems is included, thus the scheme is ready to incorporate general relativistic (GRMHD) effects. Finally, the code is parallelized under MPI directives and is able to run on all supercomputing platforms with excellent scalability.

Key words. magnetohydrodynamics (MHD) – relativity – shock waves – methods: numerical

1. Introduction

Most of the astrophysical sources of high-energy radiation and particles are believed to involve the presence of relativistic motions in *magnetized* plasmas. For example, the radio emission from extra galactic jets (especially from terminal radio lobes) or from plerion-like supernova remnants is due to synchrotron radiation produced by relativistic electrons spiraling around magnetic field lines, thus indicating the presence of significant magnetic fields. Strong magnetic fields are supposed to play an essential role in converting the energy of accreting material around super-massive black holes at the center of Active Galactic Nuclei (AGNs), into powerful relativistic jets escaping along open field lines (Begelman et al. 1984). Similar phenomena may be at work in the galactic compact X-ray sources known as microquasars (Mirabel & Rodriguez 1994). These processes in-

Send offprint requests to: L. Del Zanna
Correspondence to: L.go E. Fermi 2, 50125 Firenze, ldz@arcetri.astro.it

volve the interaction of relativistic gasdynamic flows and shocks with strong magnetic fields, which have now started to be studied via computer simulations (see Meier et al. 2001 for a review). Powerful relativistic blast shocks should also be at the origin of the still mysterious gamma-ray bursts (GRBs; Mészáros & Rees 1992).

Due to the extreme complexity and richness of the possible effects arising in relativistic plasma physics, there is a very strong interest among the astrophysical community in the development of computer codes for both relativistic hydrodynamics (RHD) and magnetohydrodynamics (RMHD), since in most cases only numerical simulations are able to cope with the evolution of such phenomena. After some early attempts based on non-conservative schemes that handled shocks with the aid of large artificial viscosity and resistivity, it is only during the last decade that conservative shock-capturing Godunov-type numerical codes, already successfully applied to gasdynamic problems, have started to be widely applied to RHD too, achieving both high accuracy in smooth regions of the simulated flow and sharp discontinuous profiles at shocks (e.g. Donat et al. 1998; Aloy et al. 1999; Del Zanna & Bucciantini 2002, and references therein). However, in spite of the success of Godunov-type RHD codes and, at the same time, of the presence of various extensions of gasdynamic schemes to classical MHD (Tóth, 2000; Londrillo & Del Zanna, 2000), to date only a couple of multidimensional RMHD schemes have been described in the literature (Komissarov, 1999; Del Zanna et al., 2002, DZ from now on). Another RMHD code, extended to general relativistic (GRMHD) effects (with given Schwarzschild or Kerr metrics), actually exists (Koide et al. 1996; 1999), although a complete set of standard numerical tests has never been published for such code, and only mildly relativistic situations are usually considered.

The reasons behind the difficulty of extending shock-capturing relativistic gasdynamic codes to the magnetic case are essentially the same encountered in building classical MHD schemes, but *amplified*, so to say, by the special relativistic effects. These difficulties may be summarized basically in two classes of problems. The first is concerned with the eigenstructure of the 1-D MHD system, which is much more complex than in the fluid case since now seven characteristic waves are involved and many different degeneracies may occur (depending on the relative orientation of the magnetic and velocity vectors). These problems of *non-strict hyperbolicity* can be cured by accurate re-normalizations of the variables, to assure their linear independence, and by introducing additional numerical viscosity in the degenerate cases. The second aspect is more crucial. The multidimensional MHD system, in conservative form, has a specific irreducible structure: the magnetic field (which is a pseudo-vector) is advanced in time by an antisymmetric differential operator, a curl, while all other variables are scalars or vectors advanced in time by a differential operator of divergence form. We notice that this basic duality in the conservation laws of the MHD system is also fully invariant under relativistic coordinate transformations: the covariant evolution equation for $\boldsymbol{B}$ splits into the classical induction equation and in the non-evolutionary solenoidal $\nabla\cdot\boldsymbol{B}=0$ condition. In numerical schemes where Godunov-type procedures, based on the divergence conservation form and on cell-centered variables, are also applied to the induction equation, it comes out that magnetic field components develop unphysical discontinuities and numerical monopoles which may grow in time. In RMHD this problem can be relevant: when the magnetic field is very strong, that is when the Alfvén velocity approaches the speed of light, the various eigenvalues collapse one onto the other and it becomes very hard, from a numerical point of view, to distinguish among different physical states: thus, even very small errors in the definition of the magnetic field components, or in the flux derivatives (where the solenoidal condition is implicitly assumed), often lead to unphysical states and to code crashing. Therefore, the proper character of the induction equation and the related preservation of the solenoidal constraint are fundamental issues in numerical RMHD.

A consistent way to handle this problem is given by the family of *constrained transport* (CT) methods (first introduced by Evans & Hawley, 1988), where the induction equation is correctly discretized to incorporate the solenoidal constraint as a main built-in property. To date, a fully consistent CT-based upwind scheme assuring exact $\nabla \cdot \boldsymbol{B} = 0$ condition has been proposed by Londrillo & Del Zanna (2000), and extended to RMHD in DZ. Starting from a finite volume formulation of the solenoidal condition and of the induction equation, as in the original CT method, general recipes are given to reconstruct (to any order of accuracy) magnetic field variables at points needed for flux computations and to formulate approximate Riemann solvers also for the induction equations in the CT form. Moreover, as an application, a third order Essentially Non-Oscillatory (ENO) *central*-type scheme was proposed and numerically validated against various tests. The so-called central schemes do not make use of time-consuming and system-dependent spectral decompositions, and linearized Riemann solvers are replaced by Lax-Friedrichs type averages over the local Riemann fan. In this way, the only characteristic quantities entering the scheme are the local fastest velocities, and also the problems related to the various degeneracies are thus avoided completely. The price to pay is just some additional numerical dissipation at contact and Alfvénic discontinuities, but the high order reconstruction is often able to compensate for these drawbacks. Finally, in DZ the ENO-CT scheme was extended to generalized orthogonal curvilinear coordinates, thus, the inclusion of General Relativity effects with a given metric, i.e. the extension to GRMHD, may be easily achieved.

In this paper, our RMHD code will be briefly described and some selected results of astrophysical interest will be shown. For more complete informations the reader is referred to Del Zanna & Bucciantini (2002) and especially to DZ.

2. The RMHD equations and the numerical scheme

As their classical MHD counterpart, the fluid part of the relativistic MHD equations retain the usual conservative form, needed for any shock-capturing scheme:

$$\frac{\partial \boldsymbol{u}}{\partial t} + \sum_{i=1}^{3} \frac{\partial \boldsymbol{f}^i}{\partial x^i} = 0.$$

Here $\boldsymbol{u}$ is the vector of conserved variables and $\boldsymbol{f}^i$ are their corresponding fluxes, along each direction, respectively given by

$$\boldsymbol{u} = [\rho u^0, w_t u^0 u^j - b^0 b^j, w_t u^0 u^0 - b^0 b^0 - p_t]^T,$$

$$\boldsymbol{f}^i = [\rho u^i, w_t u^i u^j - b^i b^j + p_t \delta^{ij}, w_t u^0 u^i - b^0 b^i]^T,$$

where we have defined $w_t = w + |b|^2$ and $p_t = p + |b|^2/2$. Here $u^\alpha = (\gamma, \gamma v^j)$ is the four-velocity, $\gamma \equiv u^0 = (1 - v^2)^{-1/2}$ is the Lorentz factor, $w = e + p$ is the relativistic enthalpy ($e = \rho + p/(\Gamma - 1)$ is the relativistic energy per unit volume for a Γ-law equation of state). The components of the magnetic four-vector are

$$b^\alpha = [\gamma(\boldsymbol{v} \cdot \boldsymbol{B}), \boldsymbol{B}/\gamma + \gamma(\boldsymbol{v} \cdot \boldsymbol{B})\boldsymbol{v}],$$

and in the fluid comoving local rest frame we simply have $b^\alpha = (0, \boldsymbol{B})$. Note the constraints $u_\alpha b^\alpha = 0$ and $|u|^2 \equiv u_\alpha u^\alpha = -1$, so that $|b|^2 \equiv b_\alpha b^\alpha > 0$ and b^α is a space-like vector, with $|b|^2 = B^2/\gamma^2 + (\boldsymbol{v} \cdot \boldsymbol{B})^2$.

On the other hand, the covariant equation for b^α splits into two parts, which happen to be exactly the same as in classical MHD (this is not surprising since Maxwell equations are Lorentz invariant). The spatial component gives the classical induction equation

$$\frac{\partial \boldsymbol{B}}{\partial t} + \nabla \times \boldsymbol{E} = 0; \quad \boldsymbol{E} = -\boldsymbol{v} \times \boldsymbol{B},$$

which is properly the time evolution equation for $\boldsymbol{B}$. Note that the spatial differential operator is in a *curl* form, rather than in a *divergence* form as the energy-momentum conservation law. This means that the evolution equation of each spatial component of $\boldsymbol{B}$ has a missing eigenspace, basically due to the antisymmetry of the electromagnetic tensor. Thus, a total of just three independent magnetic fluxes (the electric field vector components, just one in 2-D) are needed for the evolution of $\boldsymbol{B}$, while six independent fluxes were required for the momentum evolution. The other consequence of the tensor antisymmetric nature is that the time component of the covariant equation for b^α becomes the usual MHD solenoidal constraint

$$\nabla \cdot \boldsymbol{B} = 0,$$

which is *not* an evolutionary equation but a differential constraint on the spatial derivatives of $\boldsymbol{B}$. This constraint is usually regarded as just an initial condition, since the form of the induction equation assures its preservation in time. Therefore, also numerical schemes must be designed in a way that the specific divergence-free nature of the magnetic field is taken into account as a fundamental constitutive property, otherwise spurious magnetic monopoles will affect the overall solution and often the code stability itself. The CT schemes, and our specific implementation described in DZ, are the class of numerical schemes based on this property.

In the present section we briefly summarize the main points that characterize our numerical scheme:

1. A third-order TVD Runge-Kutta cycle is used for time integration (Shu & Osher, 1988). The global time step is chosen to be proportional to the inverse of the largest *fast magneto-sonic* characteristic speed present in the computational domain.
2. Point values, rather than cell averages, are used to discretize fluid conservative variables at cell centers.
3. A robust and efficient iterative scheme is used to get primitive fluid variables $(\rho, \boldsymbol{v}, p)$ from the set of conservative variables, by first projecting along the direction of the local magnetic field. The 5x5 set of equations is reduced down to just a single non-linear equation for the first time.
4. Third order Convex ENO routines (Liu & Osher, 1998; Londrillo & Del Zanna, 2000) with usual slope limiters (MinMod, Monotonized Centered) are employed for variables reconstruction at cell boundaries.
5. A two-speed solver (HLL) is used to define numerical fluxes at cell interfaces:
$$\boldsymbol{f}^{\mathrm{HLL}} = \frac{\alpha^+ \boldsymbol{f}^L + \alpha^- \boldsymbol{f}^R - \alpha^+\alpha^-(\boldsymbol{u}^R - \boldsymbol{u}^L)}{\alpha^+ + \alpha^-}.$$
Here the $\alpha^\pm$ coefficients take into account the highest speeds at the two sides of the Riemann fan, which can be estimated from the maximum and minimum eigenvalue $\lambda^\pm$ of the Jacobians at the left and right reconstructed states:
$$\alpha^\pm = \max\{0, \pm\lambda^\pm(\boldsymbol{v}^L), \pm\lambda^\pm(\boldsymbol{v}^R)\}.$$
Notice that when the local Riemann fan is symmetric, then $\alpha^+ = \alpha^- = \alpha$ and fluxe coincides with a simple local Lax-Friedrichs flux, whereas, when both fast magneto-sonic speeds have the same sign one of the $\alpha^\pm$ is zero and the HLL flux becomes a pure upwind flux, either $\boldsymbol{f}^{\mathrm{L}}$ or $\boldsymbol{f}^{\mathrm{R}}$.
6. The potential vector $\boldsymbol{A}$, for which $\boldsymbol{B} = \nabla \times \boldsymbol{A}$, is integrated in time at cell corners, rather than the staggered $\boldsymbol{B}$ components themselves. The numerical flux for A (an Hamiltonian function) is the electric field $\boldsymbol{E}$, whose HLL upwind numerical expression is a four-state function and it is provided in DZ.

3. Code validation

3.1. 2-D numerical tests

Multidimensional tests (here just 2-D, see Del Zanna & Bucciantini, 2002, for some

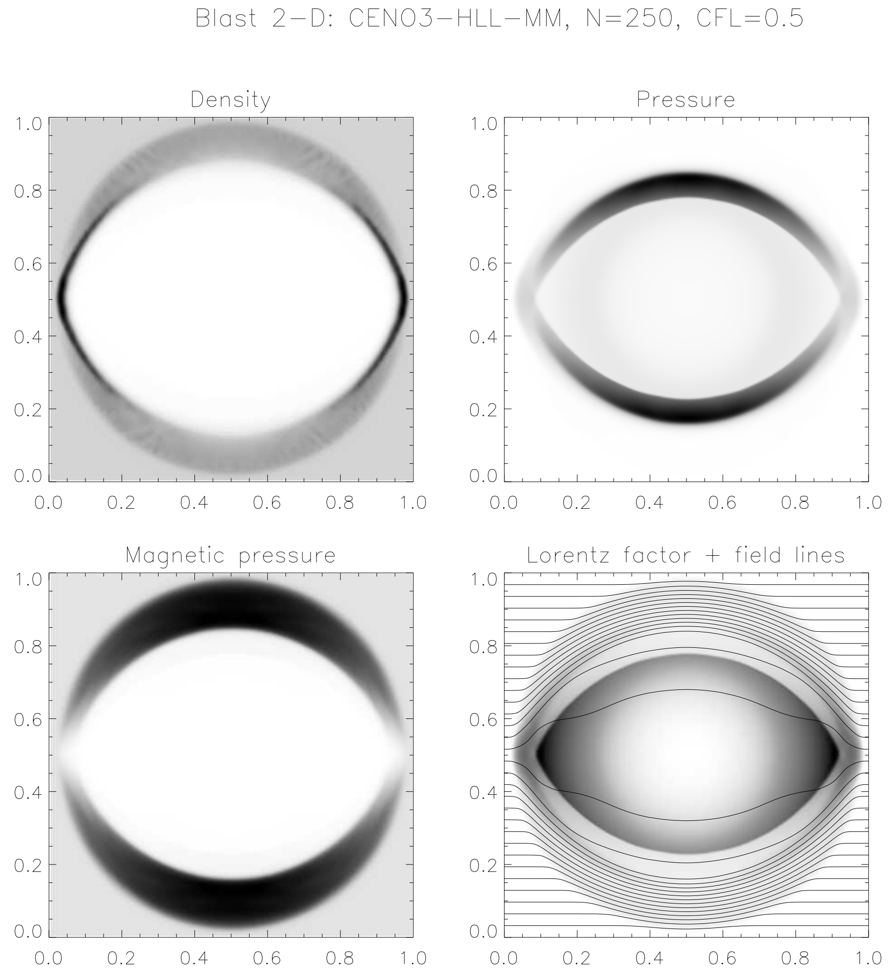

Fig. 1. A RMHD 2-D strong explosion with a pressure jump as high as 10^5. The resolution is $N_x = N_y = 250$ grid points, and the base multidimensional scheme employing HLL solver and MM limiter is used. Grayscale levels are displayed for density, kinetic pressure, magnetic pressure, and Lorentz factor (together with field lines), where $5.36 \times 10^{-3} \le \rho \le 5.79$, $0.0 < p \le 45.2$, $4.32 \times 10^{-2} \le p_m \le 72.2$, and $1.0 \le \gamma \le 4.35$.

3-D RHD tests) truly prove the robustness of the code and its accuracy in preserving $\nabla \cdot \boldsymbol{B} = 0$ in time, thus avoiding the onset of spurious forces due to the presence of numerical magnetic monopoles. The solenoidal constraint is preserved within machine accuracy, like for all CT schemes, and therefore the spatial distribution of $\nabla \cdot \boldsymbol{B}$ and its evolution in time will not be shown (however, see Londrillo & Del Zanna for proofs in classical MHD tests). The numerical parameters that may be changed in our simulations are the CFL number (here always $c = 0.5$), the reconstruction slope limiter (the Monotonized Centered, MC, or the most smearing MinMod, MM, for the multidimensional highly relativistic tests shown below; see Del Zanna & Bucciantini, 2002, for the precise definition of these limiters), the order of the reconstruction (third, with CENO routines, whenever possible), and the central-type

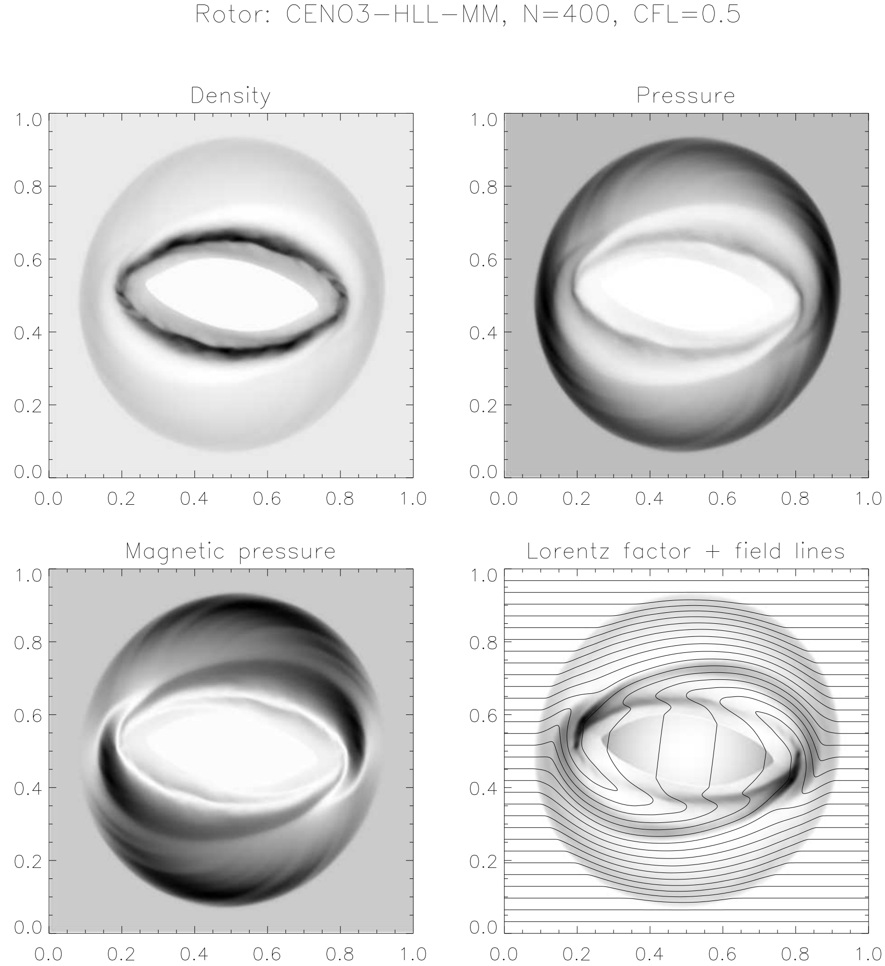

Fig. 2. The relativistic analog of the *rotor* test, with an initial maximum Lorentz factor of about 10. A high resolution ($N_x = N_y = 400$ grid points) simulation is shown, with the same numerical settings as in Fig. 1. Grayscale levels are displayed for density, kinetic pressure, magnetic pressure, and Lorentz factor (together with field lines), where $0.35 \leq \rho \leq 8.19$, $5.31 \times 10^{-3} \leq p \leq 3.88$, $3.77 \times 10^{-4} \leq p_m \leq 2.43$, and $1.0 \leq \gamma \leq 1.79$.

averaged Riemann solver (we always use the HLL solver). Concerning this last point, we have verified that HLL and LLF actually give almost identical results in all simulations. This is easily explained: in RMHD either the sound speed or the Alfvén speed are often high, especially at shocks where upwinding becomes important, so that $\alpha^+ \sim \alpha^- \sim \alpha \sim 1$ and the two fluxes tend to coincide.

In the first test we use the standard $[0,1] \times [0,1]$ Cartesian grid, here with a resolution of $N_x = N_y = 250$ grid points, and we define an initially static background with $\rho = 1.0$, $p = 0.01$ and $B_x = 4.0$. The relativistic flow comes out by setting a much higher pressure, $p = 10^3$, within a circle of radius $r = 0.08$ placed at the center of the domain. Here we use $\Gamma = 4/3$ to reduce plasma evacuation at the center. In Fig. 1 we show the situation at $t = 0.4$, when the flow has almost reached the outer boundaries. The flow speed reaches its maximum value along the x direction, $\gamma_{\max} \simeq 4.35$, because the expansion of the blast wave is not slowed down by the presence of a transverse magnetic field, as it happens along y where field lines are squeezed producing the highest magnetic pressure. Magnetized cylindrical blast wave are a nice tool to investigate the behavior of the plasma, and the robustness of the code, in a variety of degenerate cases. In this simulation we can see that, despite the absence of appropriate Riemann solvers handling the degeneracies, our code gives smooth and reasonable results in all directions.

The same numerical parameters, but with a higher resolution ($N_x = N_y = 400$), are employed in the second simulation, here adapted to the relativistic case from the classical MHD one. A disk of radius 0.1 with higher density, $\rho = 10$, rotating at high relativistic speed, $\omega = 9.95 \Rightarrow \gamma_{\max} \simeq 10.0$, the *rotor*, is embedded in a static background with $\rho = 1.0$, $p = 1.0$ and $B_x = 1.0$ ($\Gamma = 5/3$). In Fig. 2 the complicated pattern of shocks and torsional Alfvén waves launched by the rotor may be seen at the usual output time $t = 0.4$, when the central field lines are rotated of an angle of almost 90°. This magnetic braking slows down the rotor, whose maximum Lorentz at the output time is just $\gamma = 1.79$. Note how the initial high density central region has been completely swept away: the density has now its minimum ($\rho = 0.35$) at the center and the material has gone to form a thin oblong-shaped shell. In spite of the presence of very strong shear flows (again, no smoothing is applied to the disk boundary in the initial conditions), it appears that our central high order HLL solver is good enough both in providing high accuracy on smooth waves and in preventing numerical oscillations at shocks. The turbulent aspect of the high density shell should be due to the nonlinear evolution of shear-flow instabilities, since its position coincide with the transition layer where the flow changes its direction from tangential to radial.

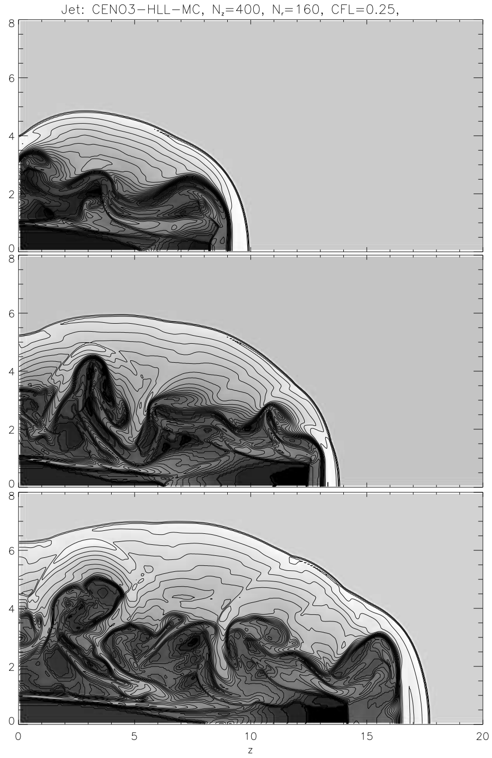

Fig. 3. A relativistic HD jet for times $t = 20$, 30, 40 in 2-D cylindrical geometry (logarithmic density contours and shades are shown). The inflow speed is $v_z = 0.99$ and the internal to external density ratio is $\eta = 1/100$, with an overall pressure equilibrium, leading to a beam relativistic Mach number of 17.9. The jet radius is assumed as length unit, corresponding to 20 computational cells ($N_z = 400$ grid points in the axial direction and $N_r = 160$ points in the radial direction). CENO3 reconstruction, HLL solver and MC limiter have been used in the simulation, with Courant number $c = 0.25$.

Finally, as a typical astrophysical test, we simulate the propagation of an axisymmetric RHD jet in 2-D cylindrical coordinates (z, r). Note that jet simulations are a very hard test for codes not based on characteristics decomposition, because of usually stronger numerical viscosity at shear layers. The domain is $0 < r < 8$ and

$0 < z < 20$, with reflective boundary conditions on the axis $r = 0$ and simple extrapolation at the other boundaries (except at $z = 0$ within the jet radius, where initial values are kept constant). At $t = 0$ a relativistic jet with $v_z = 0.99$ and density 100 times less than the surroundings (but same pressure) is located at $r \leq 1$ and $z \leq 1$. Density and velocity jumps are actually smoothed in order to reduce spurious transverse waves that appear due to numerical viscosity at the shear layer. The material is injected with a Lorentz factor $\gamma \simeq 7.1$, corresponding to a relativistic Mach number of $\mathcal{M} = \gamma v / \gamma_{c_s} c_s \simeq 17.9$. The jet evolution is followed until $t = 40$, as shown in Fig. 3, where density contours and gray shades in logarithmic scale are presented. The code settings are CENO3-HLL-MC, while the resolution employed is 400×160, corresponding to 20 grid points per jet radius. Note that the smearing of contact discontinuities, unavoidable in methods not based on characteristics decomposition, is actually small and vortices due to Kelvin-Helmoltz instabilities are nicely defined, as well as the external bow shock, the internal Mach disk and other shocks reflected off the axis. Moreover, notice the absence of the so-called *carbuncle* problem, usually manifesting as an extended *nose* in the front of the jet on the axis.

3.2. Convergence tests

In the present subsection we check the high resolution properties of the interpolation routines on smooth fields. In cases where discontinuous features are absent, these algorithms are designed to achieve third order accuracy. However, the reader might wonder whether the overall RMHD scheme itself, which is based on a rather complicated sequence of CENO3 reconstruction and derivation routines, especially in the multidimensional case, is really able to preserve global third order accuracy properties in both time and space.

To this porpouse let us study the propagation of a monochromatic relativistic circularly polarized (CP) Alfvén wave. In the limit of small amplitudes the total magnetic field strength is preserved in time, the Alfvén speed is given by $B_0/\sqrt{w_t}$ and the relation between velocity and magnetic fluctuations reduce to $\delta \boldsymbol{v} = \pm \delta \boldsymbol{B} / \sqrt{w_t}$, similarly to the classical MHD case. Define now, at $t = 0$, the various quantities in a generic cartesian reference frame (ξ, η, ζ) as $\rho = 1$, $p = 0.1$, $v_\xi = 0$, $B_\xi = B_0 = 1$, and

$$v_\eta = -B_\eta = A \cos(2\pi\xi),$$
$$v_\zeta = -B_\zeta = A \sin(2\pi\xi),$$

where we have taken $A = 0.01$. In the 1-D case we simply have $(\xi, \eta, \zeta) = (x, y, z)$, whereas in the 2-D case we consider propagation along the $x = y$ direction, so that $(\xi, \eta, \zeta) = ((x + y)/\sqrt{2}, (-x + y)/\sqrt{2}, z)$. In both cases $[0, 1]$ intervals and periodic boundary conditions have been assumed, so that after one period $t = T$ the wave should return unchanged to the initial position, as long as transverse relativistic effects can be neglected (they scale as $A^2 = 10^{-4}$). In 1-D $B_0 = 1$ and the wave period is $T = 1$, while in 2-D we take $B_0 = \sqrt{2} \Rightarrow B_{0x} = B_{0y} = 1$, so that two complete spatial periods are set along the main diagonal $x = y$ and therefore $T = 0.5$.

Third order convergence, in time and space, can thus be proved by measuring relative errors of a certain quantity, v_z in our case, at different resolutions, where the error is here evaluated as the L_1 norm of the numerical solution after one period T, compared to the initial settings. In Fig. 4 the errors are plotted in both 1-D and 2-D cases as a function of the number of grid points employed $N = N_x = N_y$, in logarithmic scale. As expected, third order accuracy is achieved, already in low resolution runs. The base scheme employed is CENO3-HLL-MM, which gives the smoothest profiles, more appropriate to wave-like features. However, we have also tested the sharper MC limiter: third order accuracy is globally preserved, but the behavior of the relative errors is more oscillatory, probably due to artificial compression that tends to sharpen somehow even sinusoidal waves.

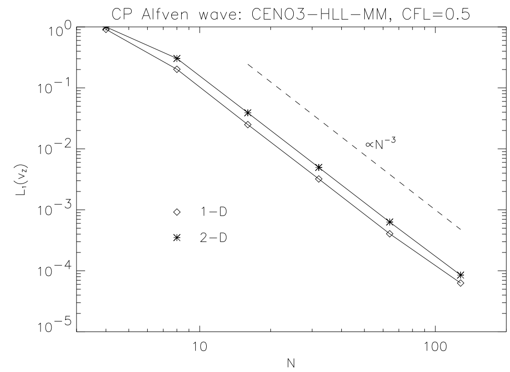

Fig. 4. Convergence test for the 1-D and 2-D CP Alfvén wave problem. Relative L_1 errors on v_z are shown in logarithmic scale. Note that the code soon achieves third order convergence in both cases. The errors in the 2-D case are larger because two periods fit on the main diagonal. The last point in the 1-D case refers to a slightly larger error than expected for perfect third order accuracy, because relativistic effects begin to appear on the wave profile and we are no longer comparing with the correct solution.

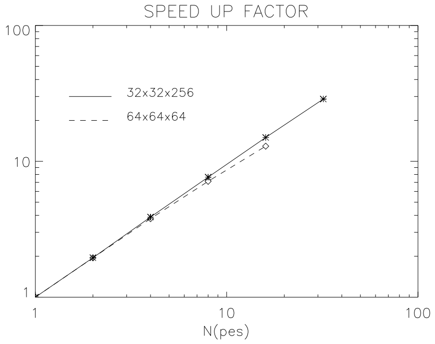

Fig. 5. The speedup factor as a function of the number of processors N, in logarithmic scale. Parallelization (with MPI) has been achieved by splitting the z domain in N sub-domains. When these have a sufficient number of grid points in z, say 10, scalability is almost perfect.

4. Code parallelization

For large 2-D and especially 3-D simulations, the code must be parallelized. This had been already done for the original MHD code (Londrillo et al., 2001), and the addition of the relativistic F90 modules has not affected the overall parallel structure of the code. Parallelization was achieved under MPI directives by splitting the z domain in N_{PE} sub-domains, where N_{PE} is the number of processors employed that can be defined at run-time, like the number of grid-points in all directions. The ghost cells technique was used for boundary conditions, so that communication among consecutive sub-domains is naturally achieved thanks to the use of *send-receive* directives. The only other two places where parallel directives are needed are I/O routines and in the definition of the global time-stepping increment dt.

In Fig. 5 the speed-up factor is shown for two different sets of resolutions. As we can see, when sufficient grid points are present in each z sub-domain, scalability is almost perfect. The data plotted refer to test runs on the Cineca Cray T3E, now dismissed. However, the use of the MPI standard makes our code portable and equivalent performances are obtained on all other Cineca platforms (IBM SP4, Beowulf Linux cluster).

5. Conclusions

The shock-capturing 3-D MHD scheme of Londrillo & Del Zanna (2000) has been applied to the special relativistic case in Del Zanna & Bucciantini (2002), for the purely hydrodynamics case, and in Del Zanna et al. (2002), for the magnetic case. This is the first higher than second order (third) upwind scheme developed for RMHD, to which high resolution Godunov-type methods have started to be applied only very recently. Instead of defining complicated linearized Riemann solvers, usually based on reconstructed characteristic fields, our scheme just uses the local fastest characteristic velocities to define a two-speed HLL-type Riemann solver. Moreover, reconstruction is applied component-wise, thus time-consuming spectral decomposition is avoided completely, in the spirit of the so-called central schemes. This is of particular importance in both MHD and RMHD, since we do not need to worry about ubiquitous degenerate cases, usually handled in Roe-type schemes by adding artificial numerical viscosity.

A main feature of our code is the correct treatment of the solenoidal constraint, which is enforced to round-off machine errors by extending the constraint transport (CT) method, originally developed for the induction equation alone, to the overall RMHD system: the flux functions are correctly defined by using the staggered magnetic field components, thus avoiding the onset of monopoles even at discontinuities. It is important to notice that, in order to obtain such results, $\nabla \cdot \boldsymbol{B}$ must be kept equal to zero at cell centers and it must be calculated by using the same staggered components which are evolved in time and the same discretizations applied to flux derivatives. Moreover, numerical fluxes based on four-state reconstructed quantities are defined for the induction equation and here applied to a two-speed central-upwind solver for the first time. In our opinion, to date our method is the only consistent application of CT to an upwind scheme for mixed systems of hyperbolic and Hamilton-Jacobi equations, like MHD and RMHD.

Particular attention has been also devoted to the numerical method needed to derive primitive variables from the set of conservative ones. The 5×5 system of nonlinear equation is reduced to just a *single* equation for the square of the velocity. This is then solved via a Newton-Raphson iterative root-finding algorithm, and analytical expressions are provided for the function whose zeroes are looked for and for its first derivative. This procedure is extremely efficient and robust, and may be used in all RMHD codes, regardless of the numerical scheme employed.

Here selected 2-D test problems, even in non-Cartesian geometries, are presented for code validation, showing accurate results and non-oscillatory profiles. The code is very robust within the limits imposed by the intrinsic numerical precision, essentially due to the fact that physical states become undistinguishable in the ultrarelativistic regime (e.g. all characteristic speeds collapse onto the speed of light), where even very small errors on the reconstruction produce fluxes that lead to unphysical states. The code has been parallelized with MPI and runs on all supercomputing platforms at CINECA, achieving very good scalability when sufficient grid points are present in each sub-domain. Finally, generalized orthogonal curvilinear coordinates are defined in the code, so our scheme may be easily extended to include General Relativity effects with a given metric.

References

Aloy, M.A., Ibañez, J.M., Marti, J.M., Müller, E., 1999, ApJS, 122, 151
Begelman, M.C., Blandford, R.D., Rees, M.J., 1984, Rev. Mod. Phys., 56, 255
Del Zanna, L., Bucciantini, N., 2002, A&A, 390, 1177
Del Zanna, L., Bucciantini, N., Londrillo, P., 2002, A&A, *in press* (DZ: *astro-ph 0210618*
Donat, R., Font, J.A., Ibañez, J.M., Marquina, A., 1998, J. Comput. Phys., 146, 58
Evans, C., Hawley, J.F., 1988, ApJ, 332, 659
Koide, S., Nishikawa, K.-I., Mutel, R.L., 1996, ApJ, 463, L71
Koide, S. Shibata, K., Kudoh, T., 1999, ApJ, 522, 727
Komissarov, S.S., 1999, MNRAS, 303, 343
Liu, X.-D., Osher, S., 1998, J. Comput. Phys., 142, 304
Londrillo, P., Del Zanna, L., 2000, ApJ, 530, 508
Londrillo, P., Del Zanna, L., Velli, M., 2001, in *Science and Supercomputing at CINECA - 2001 Report*, CINECA, Casalecchio di Reno (BO), p. 41
Meier, D.L., Koide, S., Uchida, Y., 2001, Science, 291, 84

Mészáros, P., Rees, M.J., 1992, MNRAS, 258, 41
Mirabel, I.F., Rodriguez, L.F., 1994, Nature, 371, 46
Shu, C.-W., Osher, B., 1988, J. Comput. Phys., 77, 439
Tóth, G., 2000, J. Comput. Phys., 161, 605